ADVANCED FUNCTIONAL MATERIALS
www.afm-journal.de

Engineered Metal-Loaded Biohybrids to Promote the Attachment and Electron-Shuttling between Enzymes and Carbon Electrodes

*Andoni Rodriguez-Abetxuko, Elena Romero-Ben, Aitor Ontoria, Marcos Heredero, Beatriz Martín-García, Krishan Kumar, Sergio Martín-Saldaña, Felipe Conzuelo, and Ana Beloqui**

The inorganic content and the catalytic performance pose metal-loaded enzyme nanoflowers as promising candidates for developing bioelectrodes capable of functioning without the external addition of a redox mediator. However, these protein-inorganic hybrids have yet to be successfully applied in combination with electrode materials. Herein, the synthesis procedure of these bionanomaterials is reproposed to precisely control the morphology, composition, and performance of this particular protein-mineral hybrid, formed by glucose oxidase and cobalt phosphate. This approach aims to enhance the adherence and electron mobility between the enzyme and a carbon electrode. The strategy relies on dressing the protein in a tailored thin nanogel with multivalent chemical motifs. The functional groups of the polymer facilitate the fast protein sequence-independent biomineralization. Furthermore, the engineered enzymes enable the fabrication of robust cobalt-loaded enzyme inorganic hybrids with exceptional protein loads, exceeding 90% immobilization yields. Notably, these engineered biohybrids can be readily deposited onto flat electrode surfaces without requiring chemical pre-treatment. The resulting bioelectrodes are robust and exhibit electrochemical responses even without the addition of a redox mediator, suggesting that cobalt complexes promote electron wiring between the active site of the enzyme and the electrode.

1. Introduction

The field of biocatalysis has witnessed significant progress since Cohen and Boyer established the foundations of recombinant DNA technology in 1978.[1] Protein engineering, besides enhancing the catalytic efficiency of enzymes, has been exploited for the controlled immobilization and heterogenization of the biocatalyst.[2,3] These advancements reinforce enzyme performance and broaden the scope of technologies and applications where enzymes find utility. However, it is essential to note that recombinant DNA technology, while allowing for the insertion of minor modifications, cannot significantly alter the overall composition of the protein surface. In response, alternative chemical methodologies, such as the decoration of the protein surface with tailored polymer chains, have been proposed. Notably, developing single enzyme nanogels (SENs), aiming to confine proteins within a thin polymeric nanogel, stands out as a promising approach for the comprehensive modification of the protein surface.[4,5]

The formation of organic–inorganic enzyme hybrids, namely enzyme-loaded metal organic frameworks (MOFs) or enzyme inorganic nanoflowers, is a clear example of the relevance of the composition of the surface of the protein on the overall assembly efficiency of those.[6,7] As for enzyme nanoflowers, the growth of well-defined structures resembling beautiful flowers is promoted by the ability

A. Rodriguez-Abetxuko, E. Romero-Ben, A. Ontoria, M. Heredero, K. Kumar, S. Martín-Saldaña, A. Beloqui
POLYMAT and Department of Applied Chemistry
University of the Basque Country (UPV/EHU)
Donostia-San Sebastián 20018, Spain
E-mail: ana.beloquie@ehu.eus

The ORCID identification number(s) for the author(s) of this article can be found under https://doi.org/10.1002/adfm.202400479

DOI: 10.1002/adfm.202400479

B. Martín-García
CIC nanoGUNE BRTA
Donostia-San Sebastián 20018, Spain

B. Martín-García, A. Beloqui
IKERBASQUE
Basque Foundation for Science
Bilbao 48009, Spain

F. Conzuelo
Instituto de Tecnologia Química e Biológica António Xavier
Universidade Nova de Lisboa
Oeiras 2780-157, Portugal

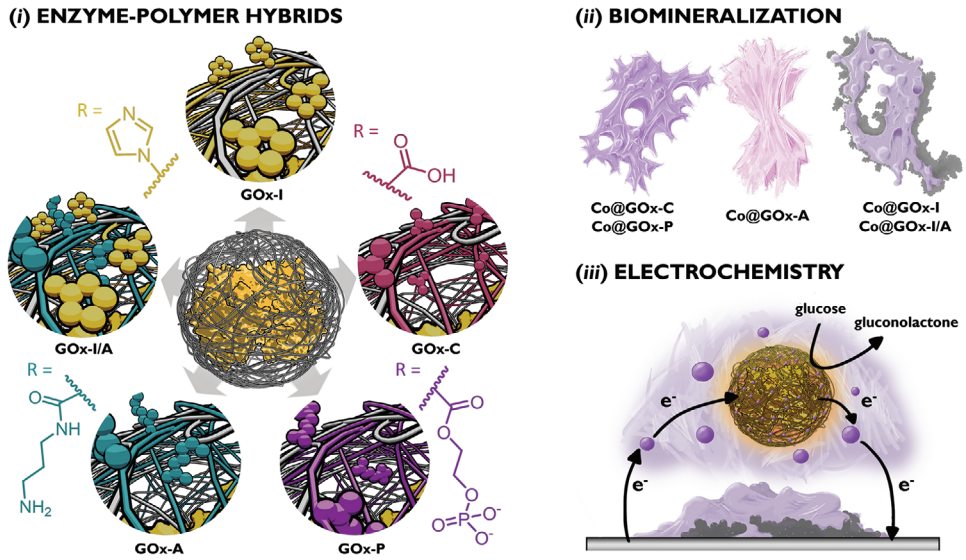

Scheme 1. The preparation of the engineered cobalt biohybrids entailed the fabrication of a single enzyme nanogel (SEN) library (*i*) with distinct polymeric mantles decorated with different chemical functionalities (R). Upon triggering the biomineralization with $Co(NO_3)_2$ in PBS, each of the functionalities (imidazole, propylamine, carboxylic acid, ethyl phosphate) leads to the formation of hybrids of varied composition, morphology, and catalytic performance (*ii*). Finally, their use for the electrochemical detection of glucose (with and without the addition of a redox mediator in solution) over a carbon electrode is tested (*iii*).

of proteins to trap and accumulate metal cations on their surface, ultimately leading to the nucleation and growth of metal phosphate minerals.[8–10] This process is regulated by metal-binding sites—specific regions on the protein surface rich in chelating amino acids, notably glutamic acid, aspartic acid, and histidine.[11,12] Formed nanostructures can exhibit outstanding catalytic performance,[13] surpassing the activity of the corresponding soluble enzyme, such as a remarkable 450% increase for laccase or up to 7260% for papain.[8,14] Further, enzyme nanoflowers demonstrate prolonged shelf-life and exceptional reusability maintained for more than five reaction cycles with minimal loss of catalytic performance.[8,15]

Copper is the predominant metal cation utilized for the fabrication of enzyme nanoflowers. The prevalent use of copper cations can be attributed to their high affinity towards the surface of proteins, along with the kinetically favored formation of copper phosphate crystals.[6] Consequently, exploring enzyme nanoflowers based on metal cations with lower avidity to bind proteins, e.g. cobalt, has been relatively overlooked, with relatively few documented examples in the literature.[9,16–21] Importantly, the formation of cobalt-based enzyme biohybrids holds great potential, given that cobalt serves as the inorganic cofactor for numerous enzymes, plays a fundamental role in catalysis, and functions as an allosteric activator.[16] The challenging assembly of cobalt phosphate enzyme nanoflowers was first addressed by López-Gallego et al., showing that only engineered proteins could be successfully biomineralized using $Co(NO_3)_2$ salts.[21] They inserted an artificial binding site based on a hung histidine tag that led to the formation of nanoflowers with acceptable protein encapsulation yields —increasing the protein loadings from 19 to 53% after 72 h of incubation.

Our interest in embedding enzymes in cobalt phosphate nanostructures extends beyond improving enzyme performance. Cobalt phosphate inorganic nanostructures are applied in direct electrochemistry owing to their excellent electrochemical properties, low cost, and environmentally friendly fabrication, being broadly employed in oxygen evolution reaction, photocatalysis, and supercapacitor applications.[22–27] Combined with functional proteins, cobalt phosphate nanostructures have been utilized for the electrochemical sensing of hydrogen peroxide and for the detection of several biomarkers.[28,29] However, implementing this hybrid electrochemical approach poses several challenges, such as (*i*) the low enzyme immobilization yields on the surface of flat electrodes, (*ii*) the poor adherence of nanoflowers on the electrodes, and (*iii*) the need for redox mediators to shuttle electrons from the biocatalyst to the electrode. Therefore, the achievement of efficient bioelectrodes requires the design of engineered cobalt-enzyme biohybrids that can effectively address the challenges exhibited by the nanomaterials synthesized through current methodologies.

In this work, we explore the engineering of cobalt biohybrids to overcome the main hurdles in implementing enzyme/cobalt phosphate-based hybrid electrochemistry. We seek to decorate the surface of the enzyme with assorted chemical functionalities that mimic natural metal-binding residues (**Scheme 1***i*). Hence, chemical functionalities from the most relevant chelating amino acids of the protein —such as imidazoles (from histidines), primary amines (lysines), and carboxylic groups (aspartic and glutamic acids)— and phosphate motifs have been strategically allocated on the protein surface using a polymeric mantle that envelops the glucose oxidase (GOx) enzyme. We hypothesize that the change in surface composition will significantly influence the assembly of the cobalt biohybrids and, in turn, will impact on their composition and morphology (Scheme 1*ii*). Finally, we have assessed cobaltbiohybrids as valuable nanomaterials for coating carbon-based electrodes and for the eventual electrochemical

Table 1. Hydrodynamic diameter (as measured by DLS), polydispersity index (PDI), and ζ-potential of SENs synthesized in this work (mean ± standard deviation; n = 3). Free GOx is measured as a reference.

Nanogel sample	Functional Monomer	Hydrodynamic diameter [nm]	PDI	ζ-potential [mV]
GOx-A	APMm	11.62 ± 1.98	0.59 ± 0.03	2.85 ± 1.76
GOx-C	AAm	7.40 ± 0.22	0.38 ± 0.02	−27.3 ± 1.23
GOx-I	VIm	8.25 ± 0.35	0.59 ± 0.07	−11.1 ± 0.18
GOx-I/A	VIm, APMm	10.09 ± 0.21	0.37 ± 0.03	6.9 ± 0.24
GOx-P	MAEPm	8.42 ± 1.47	0.52 ± 0.01	−26.4 ± 1.4
GOx	–	6.56 ± 0.33	0.15 ± 0.07	−12.03 ± 3.26

detection of glucose, also in the absence of external mediators (Scheme 1*iii*).

2. Results and Discussion

2.1. Synthesis and Characterization of the Engineered Cobalt-Loaded Biohybrids

2.1.1. Tuning the Surface of GOx with Polymeric Nanogels

GOx enzyme was selected as the model protein due to its intrinsic stability, high catalytic activity, and well-studied bioelectrochemical behavior.[30] GOx was engineered by covering its surface with a thin crosslinked polyacrylamide-based nanogel. This methodology endeavors to introduce diverse chemical functionalities in close proximity to the surface of the protein while minimizing the loss of catalytic activity (see Table S1, Supporting Information for detailed description). Hence, the GOx surface was artificially modified by the introduction of mimetic (*i*) lysines for the synthesis of GOx-A — using N-(3-Aminopropyl) methacrylamide, APMm, (*ii*) glutamic acids for GOx-C — employing acrylic acid, AAm, and (*iii*) histidines for GOx-I — using vinyl imidazole, VIm. We also designed a combined nanogel with artificial histidines and lysines (*iv*) for GOx-I/A — with APMm and VIm. Finally, (*v*) aiming to resemble a post-translational modification of the protein surface, monoacryloxyethyl phosphate functional monomer, MAEPm, was inserted in GOx-P nanogels (**Table 1**).

The success of the encapsulation was assessed through Sodium Dodecyl Sulfate-Polyacrylamide Gel Electrophoresis (SDS-PAGE, Figure S1, Supporting Information). Additionally, Dynamic Light Scattering (DLS) measured the increase in size, and ζ-potential measurements tracked changes in the surface charge of the GOx enzyme. Results are collected in Table 1 and Figure S2 (Supporting Information). The synthesis resulted in thin polymeric nanogels of ≈1–2 nm thickness. We observed that those nanogels synthesized from the positively charged monomer, APMm, exhibited the thickest shell, measuring ca. 2.5 nm. This effect could be attributed to the electrostatic attraction between APMm and the negatively charged patches of GOx at pH 6.0.[30] The accumulation and high local concentration of the APMm monomer around the protein surface likely contributed to the growth of thicker nanogels.[31] Furthermore, the introduction of APMm to the network caused a substantial change in the net surface charge, causing a shift of the ζ-potential from −14.4 to +2.8 mV. In contrast, MAEPm and AAm led to more negative ζ-potential values, measuring −26.4 and −27.3 mV, respectively.

The incorporation of the respective monomers within the polymeric nanogel was confirmed by Attenuated Total Reflectance-Fourier Transform Infrared (ATR-FTIR) spectroscopy (Figure S3, Supporting Information). In addition to the typical vibration bands from the protein, the SEN hybrids exhibited distinctive features, including the symmetrical bending vibrations of the imidazole ring at 917 cm^{-1} (observed in GOx-I and GOx-I/A), the stretching vibration corresponding to the carbonyl C═O bond of the carboxylic acid at 1710 cm^{-1} (observed in GOx-C), and the stretching vibration of the carbonyl group of the MAEP monomer at 1725 cm^{-1} (identified in GOx-P). These spectral characteristics confirm the successful integration of specific monomers into the nanogel structure, providing insight into the chemical composition of the engineered biohybrids. Therefore, we can conclude that a small library of GOx-SENs with significant variations in surface charge and composition was successfully achieved.

2.1.2. Assembly and Characterization of the Engineered Cobalt Biohybrids

Next, we ascertained the impact exerted by each inserted functionality —imidazole, primary amine, phosphate, and carboxylic acid— on the biomineralization and assembly of cobalt-loaded biohybrids. In the biomineralization process, an entropic-guided mechanism in which the protein ligands entrap metal cations is followed by a kinetically regulated formation of metal phosphates.[8] Hence, we monitored the initial stage of the biomineralization to assess the capability of each of the ligands to trap and accumulate cobalt cations. For that, we shortened the "standard" protocol from 72 to 5 h. The remaining biomineralization conditions were kept as reported in the literature, i.e. 0.1 mg mL^{-1} of protein and 1 mM of $Co(NO_3)_2$ in PBS. SENs reported in Table 1 were compared to naked GOx, used as a reference. The resulting cobalt-based biohybrids are denoted with the Co@ prefix, followed by the sample name of the SEN employed for the assembly. For instance, Co@GOx-I represents hybrids formed through Co(II) assembly using GOx nanogels with imidazole motifs as functional entities.

Efficient biomineralization is featured by high protein immobilization yields assembled within hierarchically organized cobalt phosphate layers. Here, the protein immobilization yield was evaluated by quantifying the non-bound GOx present in the supernatants after the biomineralization process (**Figure 1**A) and

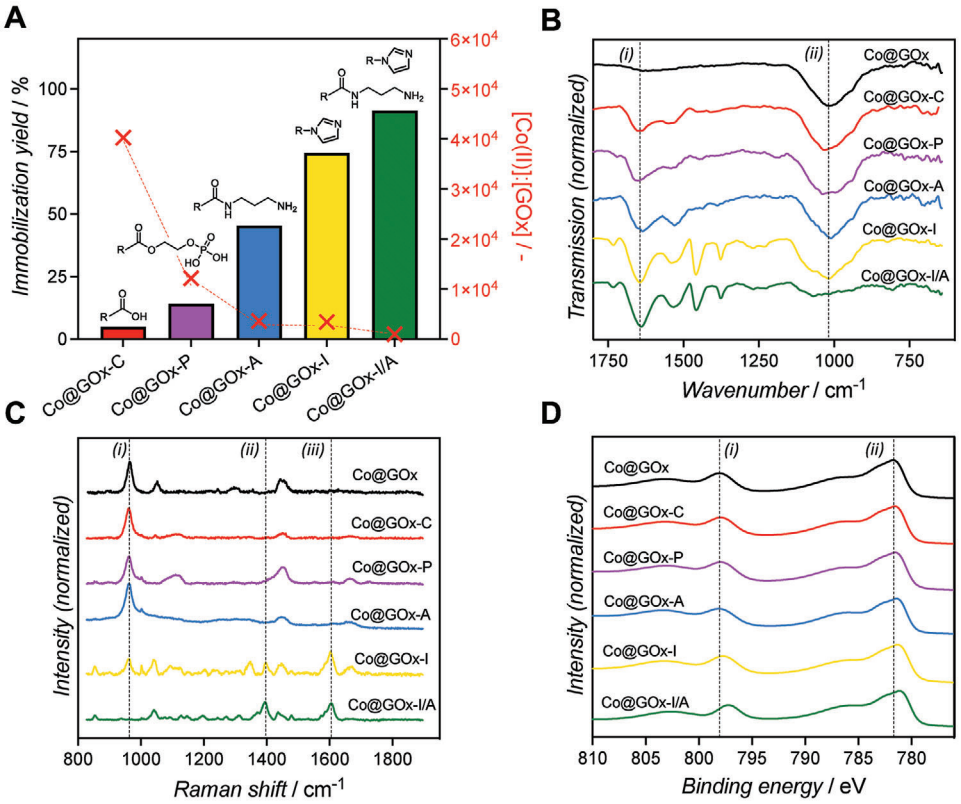

Figure 1. Characterization of the cobalt-loaded biohybrids. A) Immobilization yields (as % of offered GOx, in bars. The chemical structure of the inserted functional groups is represented on top of each of the bar) and [Co(II)]:[GOx] molar ratio measured by ICP-MS (in red crosses). B) Normalized ATR-FTIR spectra of Co@GOx samples with the relevant peaks highlighted: (i) Amide I band at ca. 1645 cm^{-1}; (ii) asymmetric and symmetric stretching vibrations typical of phosphates at ca. 1011 cm^{-1}. C) Normalized Raman spectra of Co@GOx samples with the relevant peaks highlighted: (i) the stretching vibrations of phosphates at 962 cm^{-1}; (ii) 1400 cm^{-1} deformation vibration band of CH_2 groups from proteins; and (iii) 1605 cm^{-1} band from the C=C stretching of the imidazole moiety. D) Normalized XPS spectra measured for the cobalt biohybrids zoomed in in the Co 2p region: (i) Co $2p_{1/2}$ main peak at ca. 803 eV shows a clear shift in Co@GOx-I and Co@GOx-I/A; (ii) Co $2p_{2/3}$ main peak at ca. 781 eV.

further corroborated by the UV-vis spectra of the solid precipitates (Figure S4, Supporting Information). Substantial differences were observed among all the analyzed samples. Co@GOx showed no protein load after 5 h and only 16% immobilization was achieved after 72 h of incubation. Consistent with prior research,[32] Co@GOx-I significantly improved the immobilization yield to up to 75% after just 5 h of incubation. Imidazole ligands played a crucial role in accumulating Co(II) near the protein surface, facilitating highly efficient hybrid assembly. Note that our strategy overperforms the yields obtained upon the cloning of recombinant histidine tags to the protein.[21] Interestingly, in addition to imidazole motifs, the multiple primary amines from GOx-A also gave rise to a notable enhancement in the immobilization yield, reaching 45% after 5 h of incubation. This observation underscores the previously overlooked role of amino functional groups, such as those found in lysines, as key contributors to the biomineralization process. Furthermore, we demonstrated the limited impact of multivalent carboxylic acids (present in glutamic and aspartic acids) and phosphate groups (typically found in post-translational modifications of proteins) on the overall mineralization procedure, resulting in only 14% and 5% immobilization yield for GOx-P and GOx-C, respectively, after 5 h of assembly. Consequently, these findings highlight the density of exposed histidines and lysines as the most influential residues that guide the primary stage of cobalt-driven biomineralization.

We shed light on the chemical composition of the cobalt biohybrids through additional spectroscopic techniques, including ATR-FTIR, Raman spectroscopy, Inductively Coupled Plasma-Mass Spectroscopy (ICP-MS), and X-ray Photoelectron Spectroscopy (XPS). First, the cobalt content in each biohybrid was quantified by ICP-MS. Interestingly, a reverse correlation was observed between the cobalt-to-protein molar ratio and the immobilization yield (Figure 1A – in red). Consequently, the biohybrid with the highest protein recovery yield, namely Co@GOx-I/A, exhibited the lowest cobalt-to-protein ratio. Furthermore, the relative phosphate-to-protein content was qualitatively determined from ATR-FTIR measurements (Figure 1B). While the prominent protein peaks, represented by the Amide I band, were detected at ca. 1645 cm^{-1}, a distinct band at ≈1011 cm^{-1} indicated the asymmetric and symmetric stretching vibrations typical of phosphate compounds. The phosphate ($I_{\nu[phos]}$) to protein ($I_{\nu[prot]}$) band intensity ratio provided insights into the relative phosphate and protein content within the hybrid. Notably, the imidazole ligand prevented the growth of phosphates within the hybrid, as evidenced by $I_{\nu[phos]}$: $I_{\nu[prot]}$ ratios of 0.26 and 0.90 for Co@GOx-I/A and Co@GOx-I, respectively. In contrast, the

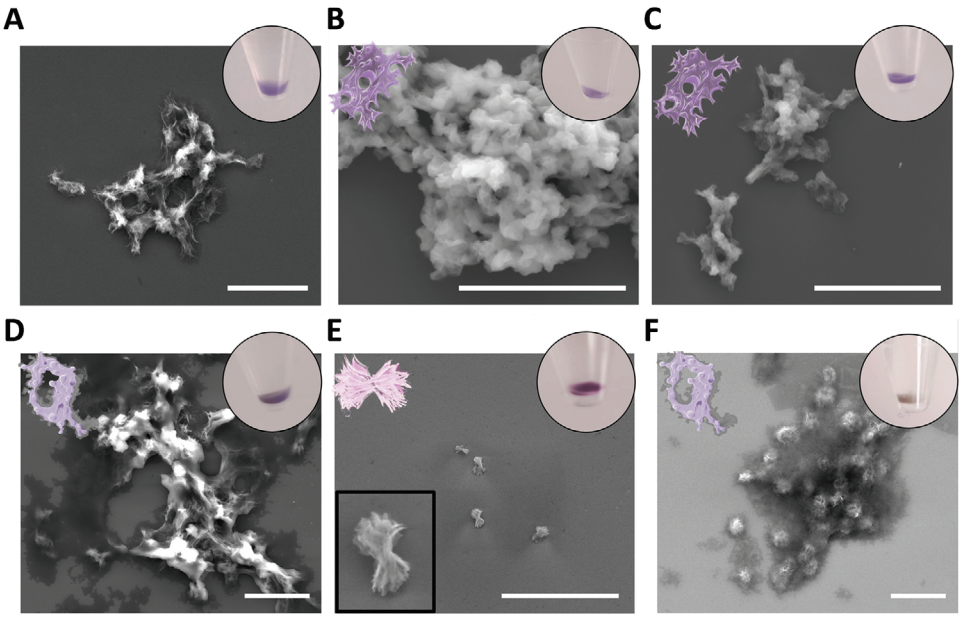

Figure 2. ESEM pictographs of the engineered cobalt biohybrids after 5 h of incubation fabricated from A) GOx (72 h); B) GOx-P; C) GOx-C; D) GOx-I; E) GOx-A (a zoomed-in image of the hybrids is provided); and F) GOx-I/A. Insets: (top right) photographs of the solid precipitates of each sample; (top left) schematic depiction of each of the hybrids used to represent the hybrids in Scheme 2. Scale bar: 5 µm.

highest ratios were measured for Co@GOx-C and Co@GOx-P samples, with 1.69 and 1.42, respectively. The unmodified protein exhibited an $I_{\nu[phos]}$: $I_{\nu[prot]}$ ratio of 6.68. Micro-Raman spectroscopy was employed to validate the results obtained from ATR-FTIR (Figure 1C) and to assess the homogeneity of the solid precipitates. Raman spectra were extracted from eight randomly defined spots on the solid structures for each biohybrid synthesized in this study (Figure S5, Supporting Information). No significant differences were observed among the spectra measured within the same sample, confirming the homogeneity of the samples. Moreover, distinctive features, including peaks at 962 and 1047 cm^{-1} from the stretching vibrations of phosphates, peaks at 1663 and 1400 cm^{-1} from proteins, and a peak at 1605 cm^{-1} from the C=C stretching of the imidazole moiety, were identified in the respective Raman spectra. This concordance further supports the consistency of the chemical composition across the samples.

The chemical composition of the biohybrids was further confirmed by XPS (Figure 1D; Tables S2 and S3, and Figure S6, Supporting Information) and Energy Dispersive X-Ray (EDX) analysis (Figure S7 and Table S4, Supporting Information). Consistent with ICP-MS results, biohybrids synthesized with APMm and VIm showed low cobalt content, ranging from 0.7 to 1.6 at%. The nitrogen atomic percentage correlated well with protein immobilization yield. Dark purple samples, namely Co@GOx, Co@GOx-P, and Co@GOx-C, displayed the highest cobalt and phosphate percentages, confirmed by a P: Co atomic ratio close to 0.66, according to XPS measurements. In contrast, VIm-containing samples exhibited lower atomic P: Co ratios, close to 0.50, suggesting a different environment for the cobalt. This observation was confirmed by the clear shift to lower binding energies presented in the Co $2p_{1/2}$ band in Co@GOx-I and Co@GOx-I/A samples (Figure 1D). Surprisingly, Co@GOx-A showed the highest phosphate-to-cobalt ratio, with a P: Co of 1.0, evidencing a unique formation mechanism, possibly based on phosphate accumulation around GOx-A due to strong electrostatic interactions. Therefore, the deep characterization of the cobalt biohybrids confirmed the achievement of nanomaterials in which the chemical environment of GOx could be significantly tuned.

2.1.3. Morphology of the Cobalt-Loaded Biohybrids

The morphology of the engineered biohybrids was further characterized using Environmental Scanning Electron Microscopy (ESEM, **Figure 2**; Figures S8–S13, Supporting Information). Biohybrids formed from negatively charged nanogels, namely Co@GOx-P and Co@GOx-C, showed similar morphological features. Both samples displayed spherical nodes of ≈1 µm, interconnected within a branched network (Figure 2B,C). These images closely resemble those obtained for Co@GOx (Figure 2A) and are similar to reported cobalt phosphate nanoflowers that are grown in the absence of protein.[22] It is noteworthy that the cobalt phosphates in the engineered biohybrids form an intricate and advanced hierarchical structure after just 5 h of incubation, in contrast to the free GOx system, which requires 72 h of incubation to achieve a similar structure. Analogous structures were observed when imidazole motifs dominated the surface of GOx; however, a thin organic veil attached to the surface of the silicon wafer support was also observed (Figure 2D).

The dark color of the Co@GOx-A solid precipitate suggested a distinct composition of the material. In contrast to previous samples, the incorporation of primary amines on the surface of GOx resulted in well-defined bow tie-like structures organized in very thin inorganic layers measuring less than 1 µm (Figure 2E; Figure S10, Supporting Information). These structures exhibited less tendency to aggregate than the rest of the samples, as

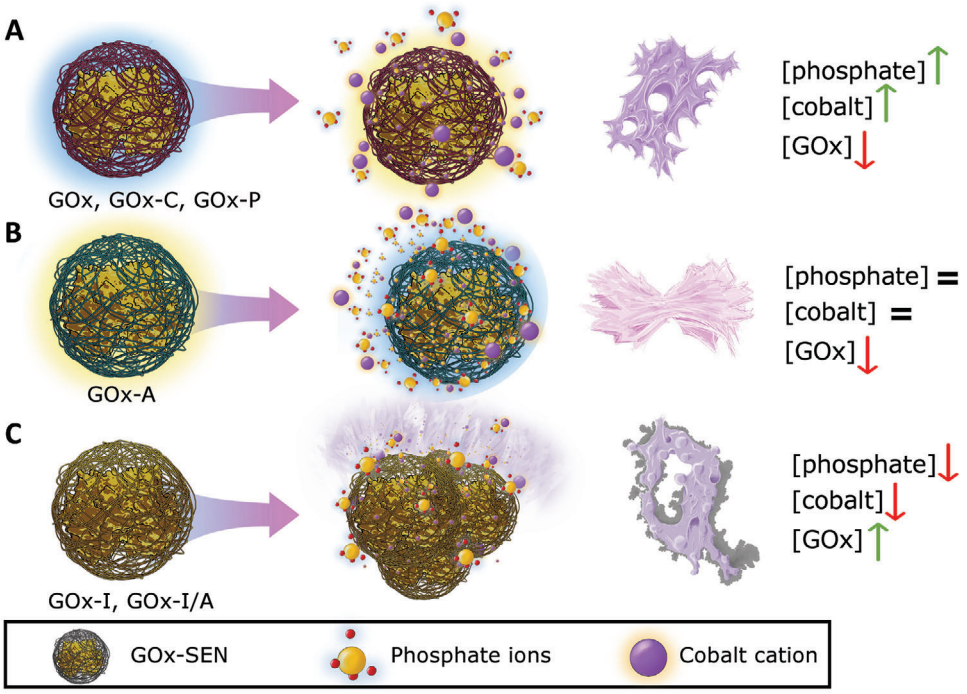

Scheme 2. Proposed growth mechanisms of the cobalt biohybrids are presented in this work. A) GOx, GOx-C, and GOx-P likely share the same assembly mechanism: the negative charge of the protein triggers the interaction of cobalt cations through electrostatic interactions, favoring the nucleation points and speeding up the biomineralization process; B) positively charged GOx-A would trigger the accumulation of phosphates around the nanogels; C) multivalent imidazole ligands present in Co@GOx-I and Co@GOx-I/A would coordinate cobalt cations, triggering the fast aggregation of the nanogels. These aggregates would generate the nucleation sites from which the cobalt phosphate is formed.

confirmed by DLS (Figure S14, Supporting Information). Finally, the biomineralization of GOx-I/A seems to be dominated by the imidazole motifs, resulting in an amorphous network similar to that found in Co@GOx-I (Figure 2F). Note that the light brown color of the Co@GOx-I/A precipitate showcases high loads of GOx (yellow color) and low content of cobalt phosphate salts, as predicted previously.

2.2. Proposed Formation Mechanism of Cobalt-Loaded Biohybrids

According to the results, it becomes evident that both the morphology and composition of the cobalt biohybrids depend on the chemical functionalities allocated on the surface of the protein. Supported by a thorough characterization of the samples, we have uncovered the underlying mechanisms that govern the assembly and biomineralization of the cobalt biohybrids (**Scheme 2**). First, we proved an inefficient assembly of non-engineered GOx due to the lack of sufficient cobalt binding sites on its surface. This situation aligns with findings in the literature for several proteins. While only a few examples describe the assembly into 3D structures, they consistently report poor protein immobilization efficiencies (maximum of 19%). Only when the surface of the protein is engineered, the protein loads are significantly improved (Table S5, Supporting Information). According to SEM images, and supported by the compositional analysis, the introduction of multivalent carboxylic acids or phosphate groups enhances the protein uptake in comparison with the unmodified protein, yet low yields were achieved compared to other hybrids. The shared morphology observed in Co@GOx, Co@GOx-P, and Co@GOx-C may indicate a common assembly mechanism based on the fast cobalt phosphate formation and the subsequent entrapment of the protein. We hypothesize that, in this case, the main force that guides the assembly lies in the electrostatic interactions between the SEN and the cobalt cation (Scheme 2A). Nanogels decorated with phosphate groups retain the cobalt cations more efficiently than those with carboxylic acids. This higher efficiency facilitates the growth of cobalt phosphate crystals more effectively, thereby accelerating the biomineralization process.

In contrast, relevant differences have been identified for the assembly mechanism of Co@GOx-A and Co@GOx-I. As for Co@GOx-A, the positive net charge induced by the multivalent primary amines on the surface favors the formation of a phosphate layer surrounding GOx-A (Scheme 2B). This could ultimately explain the highest phosphate-to-cobalt atomic ratio observed within the characterized hybrids. The growth of cobalt phosphate initiates from this phosphate layer, resulting in the development of individual structures assembled through the overlapping of nanosheets. This mechanism gives rise to the eventual formation of protein nanoflowers. To our knowledge, this is the first instance where the role of multivalent primary amines on the surface of proteins is highlighted as an effector of biomineralization for the synthesis of protein nanoflowers.

In an alternative mechanism, multivalent imidazole motifs efficiently coordinate cobalt cations and trigger the aggregation of

Table 2. Kinetic and thermostability measurements were performed for unmodified GOx and cobalt biohybrids. Co@GOx showed residual GOx activity, and kinetic parameters could not be calculated.

	GOx	Co@GOx-C	Co@GOx-P	Co@GOx-A	Co@GOx-I	Co@GOx-I/A
$^{app}K_M$ (mM)[a]	15.6 ± 0.8	22.4 ± 3.4	16.5 ± 3.3	21.6 ± 2.0	18.0 ± 1.6	17.7 ± 1.4
$^{app}k_{cat}$ (min^{-1})[b] ($\times 10^{-3}$)	34.3 ± 0.9	41.0 ± 1.1	25.0 ± 0.3	9.5 ± 0.1	32.1 ± 0.4	23.4 ± 1.0
Relative catalytic improvement[c]	–	0.94	0.64	0.51	1.30	1.82
$t_{1/2}$ at 60 °C (min)	5.5	12.0	10.5	4.5	>60	>60

[a] Biohybrids (from 0.03 to 1 nM) were mixed with growing concentrations of glucose (from 0 to 100 mM), 1 mM ABTS, and 12 nM HRP in phosphate buffer (30 mM, pH 6.0) at 37 °C; [b] A range of biohybrid concentrations (from 0 to 2 nM) were mixed with glucose, ABTS, and HRP (100 mM, 1 mM, and 12 nM, respectively) in phosphate buffer solution (30 mM, pH 6.0) at 37 °C; [c] Calculated as $^{app}k_{cat}$ (Co@GOx-X) / $^{app}k_{cat}$ (GOx-X).

SENs (Scheme 2C).[33,34] This primary assembly accumulates the enzyme nanogels that are crosslinked by cobalt cations, generating new nucleation sites for the formation of cobalt phosphate around the aggregates. This mechanism explains the high immobilization yields achieved and the low phosphate concentration found in the sample. Therefore, the use of imidazole units accelerates the assembly procedure, which limits the formation of structured flower-like morphologies under tested conditions. Cobalt phosphate salts would eventually grow from the SEN aggregates, which would also serve as nucleation points. Finally, Co@GOx-I/A exhibits a related assembly mechanism dominated by the presence of imidazole units.

2.3. Biocatalytic Performance of Cobalt-Loaded Protein Biohybrids

2.3.1. Effect of the Composition and the Morphology on the Kinetic Parameters of the Biohybrids

We aimed to determine the influence of the composition and morphology of the biohybrids on their kinetic performance. For this purpose, we measured the glucose oxidase activity for each biohybrid. Samples were added to a reaction mixture that contained glucose as substrate and horseradish peroxidase (HRP) and 2,2′-azino-bis(3-ethylbenzothiazoline-6-sulfonic acid (ABTS) as H_2O_2 formation reporter (see Supporting Information for further details). **Table 2** compiles all the kinetic parameters obtained for the protein biohybrids, along with those for the soluble GOx, which was measured as a reference (Figures S15 and S16, Supporting Information).

The apparent Michaelis-Menten constant ($^{app}K_M$) of the cobalt biohybrids was slightly higher than that measured for unmodified GOx. This effect was already observable in the respective SENs (Figures S17 and S18, and Table S6, Supporting Information). Therefore, the increase in $^{app}K_M$ could be attributed to the restrictions imposed by the entrapment of the enzymes within the polymeric layer. Interesting conclusions can be drawn from the analysis of the apparent turnover frequency ($^{app}k_{cat}$) of the samples. The formation of the heterogeneous hybrids led to a reduction in the $^{app}k_{cat}$ of the cobalt biohybrids with the highest inorganic content in their composition, as expected. We observed that only Co@GOx-A nanoflowers experience a prompt decay in $^{app}k_{cat}$ when compared to the soluble, non-modified GOx, decreasing from 34.3×10^3 to 9.5×10^3 min^{-1}. This effect can be attributed to the combined action of two factors. The corresponding SEN, GOx-A, possesses the thickest polymeric layer among the samples, leading to relevant diffusion issues, as denoted by the decrease in $^{app}k_{cat}$ to 18.6×10^3 min^{-1}. Moreover, the phosphate content and the morphology of the samples, with stacked layered sheets, could impose additional diffusion constraints on the hybrid. In contrast, the GOx-C and GOx-P nanogels did not manifest apparent diffusion issues, with $^{app}k_{cat}$ of 43.82×10^3 and 38.84×10^3 min^{-1}, respectively. The heterogenization of the samples resulted in a significant decrease in $^{app}k_{cat}$ for Co@GOx-P — 25.0×10^3 min^{-1} which was not observed for Co@GOx-C — 41.0×10^3 min^{-1}. We hypothesize that this effect is due to the different stages of biomineralization of both samples. In Co@GOx-P, protein nanogels are surrounded by thicker and more dense cobalt phosphate crystals, potentially causing strong diffusional issues in the system.

Surprisingly, we observed a slight increase in $^{app}k_{cat}$ of samples containing imidazole upon heterogenization (Table 2). Hence, Co@GOx-I and Co@GOx-I/A experienced improvements of 1.3 and 1.8 times, respectively, in $^{app}k_{cat}$ compared to their corresponding SENs. This enhancement in activity is hypothesized to be linked to the high protein concentration within these biohybrids, coupled with the low inorganic content present in their composition. Consequently, although the 3D structure of typical nanoflowers is compromised in Co@GOx-I and Co@GOx-I/A, the minimal inorganic content contributes positively to catalysis, rendering these materials compelling candidates for further characterization.

2.3.2. Assessment of the Robustness of the Biohybrids

We evaluated the thermostability of both soluble GOx and the hybrids by subjecting the samples to incubation at 65 °C for 60 min (Figure S19, Supporting Information). Native GOx, with a thermal denaturation transition temperature of 55 °C,[35] exhibited a $t_{1/2}$ of 5.5 min (Table 2). Samples engineered with imidazole motifs demonstrated exceptional stability, maintaining up to 80% of catalytic activity over an hour at 65 °C. Yet, the remaining cobalt biohybrids exhibited a modest increase in $t_{1/2}$.

The resistance to denaturation in the presence of organic solvents is also a desirable feature for enzyme hybrids. In this context, the most thermostable samples, namely Co@GOx-I and Co@GOx-I/A, were immersed in acetonitrile and 2-isopropanol (2-iPr) to assess the resistance of GOx denaturation under these conditions (Figure S20, Supporting Information). We observed that the GOx activity was conserved above 50% when incubated in

2-iPr. Importantly, the catalytic performance of the enzyme was not significantly impaired in the presence of acetonitrile.

With the assessment of the stability, we can state that cobalt-driven crosslinking of the SENs that occurs in Co@GOx-I and Co@GOx-I/A, significantly stabilizes the enzyme when exposed to high temperatures and organic solvents. On the contrary, the growth of the cobalt phosphate around Co@GOx-P and Co@GOx-C leads to labile structures. This weak interaction might be reinforced by prolonged biomineralization times, which would, in turn, exert a detrimental effect on the activity of the biohybrids due to diffusional issues.

2.4. Bioelectrochemistry

Motivated by the unique composition and unparalleled catalytic performance exhibited by the cobalt biohybrids, we evaluated their potential as electrochemical glucose hybrid sensors. The cobalt biohybrids were deposited onto carbon electrodes through a simple drop-casting approach (see Supporting Information for details). Following the removal of unbound material, cyclic voltammetry (CV) was employed for characterization in the absence and the presence of ferrocene methanol as a soluble redox mediator. The results, depicted in **Figure 3A**, reveal that Co@GOx-P, Co@GOx-C, and Co@GOx-A exhibited no response upon the introduction of glucose and the redox mediator, yielding a signal identical to that measured for the unmodified electrode. Intriguingly, the electrodes coated with Co@GOx-I and Co@GOx-I/A demonstrated a notable anodic catalytic response, indicating successful deposition of the biohybrids on the electrode surface. We propose that the strong adhesion between imidazole-containing biohybrids and carbon electrodes results from the joint action of assorted non-covalent interactions, such as hydrogen bonds, π–π stacking interactions, and hydrophobic interactions, between imidazole-SENs and the carbon surface. The coatings were robust, with only minimal current loss detected after three washing and measurement cycles (Figure S21, Supporting Information). This is relevant, considering that rather flat electrode surfaces (glassy carbon) were used. Consequently, the engineered composition and morphology of Co@GOx-I and Co@GOx-I/A facilitate the straightforward deposition and immobilization of the biohybrids on carbon electrodes. This one-pot coating strategy represents a significant advancement in enzyme-based bioelectrochemistry, obviating the need for additional chemical modifications to the electrode and substantially enhancing the enzyme load.

The utilization of protein nanoflowers for direct electrochemistry is an attractive prospect due to their metal-protein composition.[36] However, to our knowledge, there are no precedents wherein the metal cation constituents of protein nanoflowers are harnessed as mediators for promoting electron transfer (ET) between the electrode and the catalytic site of redox enzymes. Instead, metal cations-driven ET has been achieved by designing multilayered architectures on the electrode, in which metal redox centers are conveniently configured to promote the wiring between the electrode surface and redox-active proteins.[37,38] Here, we investigated the ET capabilities of the small library of cobalt biohybrids synthesized in this work. Surprisingly, we observed that, while no signal could be detected for the rest of the samples (Figure S22, Supporting Information), Co@GOx-I and Co@GOx-I/A exhibited a measurable signal starting at + 0.2 V upon the addition of glucose (Figure 3B). Under the same conditions, the signal provided by Co@GOx-I doubled the signal retrieved from Co@GOx-I/A. It is important to note that the catalytic wave for glucose oxidation of our coated bioelectrodes started at applied potentials of 0.2 V versus $Ag/AgCl/KCl_{sat}$, enabling the detection at applied potentials as low as + 0.3 V versus $Ag/AgCl/KCl_{sat}$ in the absence of a redox mediator in solution. This feature is relevant to ensure the selectivity of the attained response so that the contribution of other species present in the sample to the electrochemical response is minimized. These findings suggest that imidazole-containing cobalt biohybrids enable the wiring of electrons between the carbon electrode and the active site of the protein through the available cobalt cations. In order to demonstrate our hypothesis, further experiments that certified the enzymatic catalysis as the source of the detected signal and underscored the significance of the cobalt cations on the electron wiring were performed.

To enhance the current response, we deposited an increasing amount of Co@GOx-I biohybrid, specifically 2, 3, 4, and 6 µL of a 0.37 mg mL^{-1} solution (Figure 3C,D). Electrodes modified with 4 µL and 6 µL exhibited a lower response for glucose conversion (data not shown), likely due to the formation of a dense film that compromises molecular diffusion. Optimal results were achieved with 3 µL of Co@GOx-I. Because O_2 is the natural electron acceptor during enzymatic catalysis, the responses were also investigated after the removal of ambient oxygen from the electrolyte solution. The signals obtained under anaerobic conditions were only between 1.2 and 1.4 times higher than in the presence of O_2 (Figure 3C,D). The occurrence of relevant catalytic responses even in the presence of oxygen confirmed an effective shuttle of electrons between the active site of the enzyme and the electrode due to the intimate contact of cobalt complexes with the entrapped enzymes.

Amperometric measurements were used for additional characterizations toward glucose conversion, delivering a linear response at low glucose concentrations comprised between 0.5 and 6 mM (Figure 3E) and a limit of detection of ca. 150 and 200 µM of glucose for the electrodes deposited with 3 and 2 µL, respectively. Finally, we evaluated the dependence of the catalytic current at increasing glucose concentrations, from 0 to 40 mM, by applying a constant voltage of 0.5 V. As observed in Figure 3F, the current response showed a typical Michaelis-Menten profile, with an $^{app}K_M$ of ca. 7 mM.

Several reports have demonstrated the cobalt-driven oxidation of glucose, which would provide a non-enzymatic electrochemical response in our system.[22,39,40] To prove that the signal detected by Co@GOx-I and Co@GOx-I/A was mediated by the enzyme, we fabricated cobalt biohybrids embedded with a different protein, an ω-transaminase from *Halomonas elongata* (HeWT). As our approach is protein sequence-independent, we applied the herein-reported synthesis conditions to achieve the Co@HeWT-I cobalt-loaded biohybrid with similar morphological features to those obtained for GOx (Figure S23A,B). Upon the immersion of a carbon electrode coated with Co@HeWT-I in a glucose solution, no CV response was retrieved, neither in the presence nor in the absence of a redox mediator (Figure S23C, Supporting Information). Furthermore, we studied the possibility of

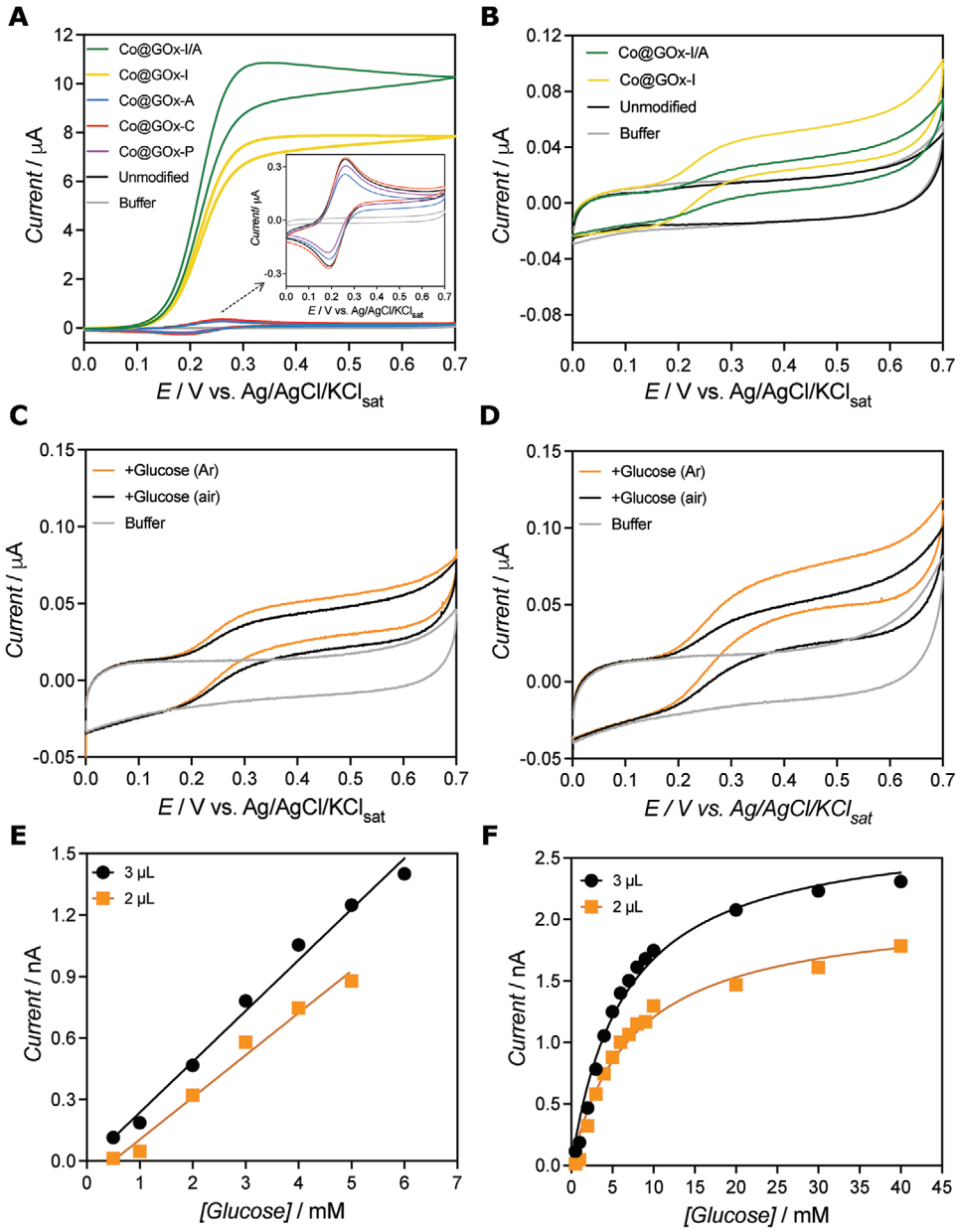

Figure 3. CV measurements were performed with cobalt biohybrids coated glassy carbon electrodes for glucose detection. A) CV measurements for the set of cobalt biohybrids in the presence of glucose (10 mM) and ferrocene methanol (100 µM). Measurements monitored for Co@GOx-P, Co@GOx-C, and Co@GOx-A coated electrodes are zoomed in for clarity. Unmodified electrodes in the presence of ferrocene methanol (Unmodified, black) and modified electrodes in the absence of redox mediator in solution (Buffer, grey) were tested as controls; B) CV measurements of Co@GOx-I and Co@GOx-I/A in the presence of glucose (10 mM) and in the absence of the soluble redox mediator; C and D) CV responses upon the deposition of 2 µL (in C) or 3 µL (in D) of Co@GOx-I onto the carbon electrodes. The modified electrodes were measured under ambient conditions or the exclusion of O_2. E) Measurement of the linear response in the 0 to 6 mM glucose concentration range for electrodes coated with 2 and 3 µL of sample. F) Response of the coated electrodes (2 and 3 µL) over a larger glucose concentration range and fitting of the obtained responses to a Michaelis-Menten model. Measurements in B, C, D, E, and F were performed without the redox mediator in solution.

using other cations, such as copper, to enable electron wiring. For that, copper-loaded biohybrids were fabricated from GOx-I sample (Figure S24A–C, Supporting Information). In this case, no catalytic current response was achieved upon the immersion of Cu@GOx-I coated electrodes in a glucose solution (Figure S24D,E, Supporting Information), emphasizing the suitability of cobalt for electrochemical applications. Finally, as the last control experiment, we removed the contribution of cobalt phosphate salts to the measurements. For that, we triggered the aggregation of GOx-I with Co(II) cations in a Tris-HCl buffer — instead of PBS that was used for previous experiments. These biohybrids exhibited only a minor catalytic response (Figure S25, Supporting Information) in the absence of the soluble redox mediator due to the poor stability of the coating compared to the samples

fabricated in the presence of phosphates. With this set of experiments, we demonstrate the enzyme-mediated oxidation of glucose and we underscore the role of cobalt phosphate to stabilize the bioactive coating and to serve as an electron shuttle for the detection of glucose in our bioelectrodes.

3. Conclusion

In this work, we have shown a strategy to tune the composition and morphology of enzyme-inorganic biohybrids based on the modification of the protein surface with multivalent chemical groups. The covering of the surface of GOx with carboxylic acids or phosphate groups speeds up the biomineralization process. Interestingly, despite achieving a similar morphology, the engineered biohybrids exhibit higher protein loads than the free protein. The role of the primary amines in the assembly and precipitation of inorganic biohybrids is herein outlined. The introduction of multiple primary groups on the surface of the protein significantly modifies the morphology and composition of the biohybrids. Positively charged protein-polymer hybrids can embed higher amounts of phosphates and protein loads than negatively charged enzyme nanogels. However, the positive charge surrounding the protein detrimentally affects the catalytic performance of the biohybrid. On the contrary, the decoration with imidazole entities significantly improved the use of the cobalt biohybrids as biocatalysts at the expense of losing the typical nanoflower-like structures. Combined with primary amines, the highest protein loadings and lowest inorganic content were achieved. This composition diminished the diffusional issues of the hybrids and, in turn, increased the stability and robustness of the GOx enzyme.

Finally, the imidazole-containing cobalt biohybrids can adhere to carbon electrodes efficiently. These bioelectrodes can be effectively used for electrochemical glucose detection in the presence and absence of redox mediators in solution. The cobalt complexes directly shuttle the electrons between the enzyme active site and the electrode, which is detected at applied potentials as low as 0.3 V versus $Ag/AgCl/KCl_{sat}$, reducing the background of the measurements. Therefore, we offer a universal methodology to fabricate cobalt biohybrids that are presented as candidates for redox sensors with high protein loads and that avoid the need for additional redox mediators.

Supporting Information

Supporting Information is available from the Wiley Online Library or from the author.

Acknowledgements

A.R.A. and E.R.B. contributed equally to this work. A.R.A. and E.R.B. shared co-authorship to this article. We thank Prof. Francesca Paradisi and Dr. Ana I. Benitez-Mateos for sharing the HeWT enzyme. A.B. gratefully acknowledges the financial support from the Spanish Research Agency (AEI) for the financial support (PID2022-142128NB-I00 funded by MCIN/ AEI/10.13039/501100011033/ and by the "European Union NextGenerationEU/PRTR"; RYC2018-025923-I from RyC program – MCIN/ AEI /10.13039/501100011033 and FSE "invierte en tu futuro"), BBVA Foundation – IN[21]_CBB_QUI_0086, and UPV/EHU- GIU21-033). K.K. thanks JdC Grant FJC2021-047607-I funded by MCIN/AEI/ 10.13039/501100011033. F.C. acknowledges FCT – Fundação para a Ciência e a Tecnologia, I.P. for the researcher contract 2022.05842.CEECIND/CP1725/CT0001 under the Scientific Employment Stimulus – Individual Call 2022. B.M.-G. thanks to support from the "Ramón y Cajal" Program by the Spanish MCIN/AEI (grant no. RYC2021-034836-I) and IKERBASQUE HYMNOS project

Conflict of Interest

The authors declare no conflict of interest.

Data Availability Statement

The data that support the findings of this study are available from the corresponding author upon reasonable request.

Keywords

bioelectrochemistry, electron shuttle, protein hybrids, protein nanoflowers, protein-polymer hybrids

Received: January 9, 2024
Revised: March 4, 2024
Published online: March 15, 2024

[1] S. N. Cohen, *Proc. Natl. Acad. Sci. USA* **2013**, *110*, 15521.
[2] Y. Zhang, J. Ge, Z. Liu, *ACS Catal.* **2015**, *5*, 4503.
[3] A. A. Caparco, D. R. Dautel, J. A. Champion, *Small* **2022**, *18*, 2106425.
[4] X. Jia, L. Wang, J. Du, *Nano Res.* **2018**, *11*, 5028.
[5] M. Yan, J. Ge, Z. Liu, P. Ouyang, *J. Am. Chem. Soc.* **2006**, *128*, 11008.
[6] M. Zhang, Y. Zhang, C. Yang, C. Ma, J. Tang, *Chem. Eng. J.* **2021**, *415*, 129075.
[7] S. Dutta, J. Kim, P. H. Hsieh, Y. S. Hsu, Y. V. Kaneti, F. K. Shieh, Y. Yamauchi, K. C. W. Wu, *Small Methods* **2019**, *3*, 1900213.
[8] J. Ge, J. Lei, R. N. Zare, *Nat. Nanotechnol.* **2012**, *7*, 428.
[9] K. H. Kim, J. M. Jeong, S. J. Lee, B. G. Choi, K. G. Lee, *J. Colloid Interface Sci.* **2016**, *484*, 44.
[10] Z. Lei, C. Gao, L. Chen, Y. He, W. Ma, Z. Lin, *J. Mater. Chem. B* **2018**, *6*, 1581.
[11] J. Gao, H. Liu, C. Tong, *Inorg. Chem.* **2023**, *62*, 13812.
[12] S. Escobar, S. Velasco-Lozano, C. H. Lu, Y. F. Lin, M. Mesa, C. Bernal, F. López-Gallego, *J. Mater. Chem. B* **2017**, *5*, 4478.
[13] Z. Lin, Y. Xiao, Y. Yin, W. Hu, W. Liu, H. Yang, *ACS Appl. Mater. Interfaces* **2014**, *6*, 10775.
[14] L. Liang, X. Fei, Y. Li, J. Tian, L. Xu, X. Wang, Y. Wang, *RSC Adv.* **2015**, *5*, 96997.
[15] H. J. Cheon, M. D. Adhikari, M. Chung, T. D. Tran, J. Kim, M. Il Kim, *Adv. Healthcare Mater.* **2019**, *8*, 1801507.
[16] L. Zheng, Y. Sun, J. Wang, H. Huang, X. Geng, Y. Tong, Z. Wang, *Catalysts* **2018**, *8*, 468.
[17] Y. Song, J. Gao, Y. He, L. Zhou, L. Ma, Z. Huang, Y. Jiang, *Ind. Eng. Chem. Res.* **2017**, *56*, 14923.
[18] K. Wu, Y. Zhang, Q. Sun, Y. Chai, Q. He, X. Zhou, X. He, H. Ji, *Enzyme Microb. Technol.* **2019**, *131*, 109386.
[19] Z. Wang, Y. Liu, X. Dong, Y. Sun, *ACS Appl. Mater. Interfaces* **2021**, *13*, 49974.
[20] G. Cao, J. Gao, L. Zhou, Y. He, J. Li, Y. Jiang, A. C. S. Appl, *Nano Mater.* **2018**, *1*, 3417.
[21] F. López-Gallego, L. Yate, *Chem. Commun.* **2015**, *51*, 8753.

[22] P. P. Tomanin, P. V. Cherepanov, Q. A. Besford, A. J. Christofferson, A. Amodio, C. F. McConville, I. Yarovsky, F. Caruso, F. Cavalieri, *ACS Appl. Mater. Interfaces* **2018**, *10*, 42786.
[23] M. Z. Iqbal, J. Khan, S. Alam, R. Ali, M. J. Iqbal, A. M. Afzal, S. Aftab, *Int. J. Energy Res.* **2021**, *45*, 18658.
[24] R. Zhang, G. Van Straaten, V. Di Palma, G. Zafeiropoulos, M. C. M. Van De Sanden, W. M. M. Kessels, M. N. Tsampas, M. Creatore, *ACS Catal.* **2021**, *11*, 2774.
[25] H. Kim, J. Park, I. Park, K. Jin, S. E. Jerng, S. H. Kim, K. T. Nam, K. Kang, *Nat. Commun.* **2015**, *6*, 8253.
[26] V. Vinothkumar, C. Koventhan, S. M. Chen, M. Abinaya, G. Kesavan, N. Sengottuvelan, *Ceram. Int.* **2021**, *47*, 29688.
[27] X. Ji, R. Zhang, X. Shi, A. M. Asiri, B. Zheng, X. Sun, *Nanoscale* **2018**, *10*, 7941.
[28] J. Liu, M. Zheng, P. Zhang, Y. Shang, J. Zheng, W. Bai, *J. Electroanal. Chem.* **2017**, *799*, 270.
[29] L. He, S. Zhang, H. Ji, M. Wang, D. Peng, F. Yan, S. Fang, H. Zhang, C. Jia, Z. Zhang, *Biosens. Bioelectron.* **2016**, *79*, 553.
[30] S. B. Bankar, M. V. Bule, R. S. Singhal, L. Ananthanarayan, *Biotechnol. Adv.* **2009**, *27*, 489.
[31] A. Beloqui, A. Y. Kobitski, G. U. Nienhaus, G. Delaittre, *Chem. Sci.* **2018**, *9*, 1006.
[32] A. Rodriguez-Abetxuko, M. C. Morant-Miñana, F. López-Gallego, L. Yate, A. Seifert, M. Knez, A. Beloqui, *Adv. Funct. Mater.* **2018**, *28*, 1803115.
[33] A. Rodriguez-Abetxuko, M. C. Morant-Minana, M. Knez, A. Beloqui, *ACS Omega* **2019**, *4*, 5172.
[34] A. Rodriguez-Abetxuko, D. Sánchez-deAlcázar, A. L. Cortajarena, A. Beloqui, *Adv. Mater. Interfaces* **2019**, *6*, 1900598.
[35] A. Zubrik, A. Musatov, M. Stupa, E. Sedla, **2004**, *279*, 47601.
[36] C. Tong, H. Liu, Y. Mo, J. Li, X. Liu, L. Pang, *Biochem. Eng. J.* **2023**, *193*, 108860.
[37] M. Jacquet, M. Izzo, S. Osella, S. Kozdra, P. P. Michalowski, D. Golowicz, K. Kazimierczuk, M. T. Gorzkowski, A. Lewera, M. Teodorczyk, B. Trzaskowski, R. Jurczakowski, D. T. Gryko, J. Kargul, *Nanoscale* **2021**, *13*, 9773.
[38] M. Izzo, S. Osella, M. Jacquet, M. Kiliszek, E. Harputlu, A. Starkowska, A. Łasica, C. G. Unlu, T. Uśpieński, P. Niewiadomski, D. Bartosik, B. Trzaskowski, K. Ocakoglu, J. Kargul, *Bioelectrochemistry* **2021**, *140*, 107818.
[39] X. Wang, M. Wang, S. Feng, D. He, P. Jiang, *Inorg. Chem. Front.* **2019**, *7*, 108.
[40] L. Xiao, Q. Chen, L. Jia, Q. Zhao, J. Jiang, *Sens. Actuators, B* **2019**, *283*, 443.